Consortium

for

Small-Scale Modelling

Technical Report No. 3

A Scheme for Monotonic Numerical Diffusion in the LM

by

G. Doms

November 2001

DOI: 10.5676/DWD_pub/nwv/cosmo-tr_3

Deutscher Wetterdienst

MeteoSwiss

Ufficio Generale per la Meteorologia

Hellenic National Meteorological Service

Amt für Wehrgeophysik

Il Servicio Meteorologico Regionale di ARPA

www.cosmo-model.org

Editors: G. Doms and U. Schättler, Deutscher Wetterdienst, P.O. Box 100465, 63004 Offenbach, Germany
Printed at Deutscher Wetterdienst, Offenbach am Main

A Scheme for Monotonic Numerical Diffusion in the LM

Günther Doms

Deutscher Wetterdienst, Abteilung Meteorologische Analyse und Modellierung,
Frankfurter Str. 135, D-63067 Offenbach am Main, Germany
guenther.doms@dwd.de

1. Introduction

Numerical weather prediction (NWP) models as well as other simulation models of atmospheric flow often apply numerical or computational smoothing in order to control small scale noise at or near the two grid interval ($2\Delta x$) wavelength. As these scales cannot be resolved adequately by the discretized dynamics, they have to be damped since otherwise large errors in the numerical solution can arise.

Numerical noise of such type is continuously generated by numerical dispersion, especially within the Leapfrog time integration using centred difference operators for advection as, e.g., in the current operational version of the Lokal-Modell (LM). Also, weak nonlinear numerical instabilities resulting from aliasing can contribute to the generation of small-scale noise, and physical processes, which in general act discontinuous at single grid points, will always introduce noise at the $2\Delta x$-scale. The formation of non-resolvable small-scale structures will also arise from topographical forcing and from surface inhomogeneities.

High-order scale-selective spatial filters can be applied to remove small-scale noise from the numerical solution (Shapiro, 1975, and Raymond, 1988). But most NWP models use computationally more efficient high-order numerical diffusion schemes to provide a scale selective control of small-scale noise. These schemes, however, have unwanted side effects. First, they are in general not monotonic and thus can introduce negative values on fields that are positive definite as, e.g., the cloud water content or the specific humidity. Second, they introduce noise by themselves on the resolvable scales via the so-called Gibbs phenomenon.

Another problem of using high-order numerical diffusion schemes in NWP models arises from the fact that smoothing is usually applied as a horizontal diffusion, that is along terrain-following model layers and not explicitly in the vertical direction. A full 3-D formulation would have to take into account a large number of metric terms from the terrain-following coordinate transformation and thus is too expensive for an operational application. In case of high-resolution modelling with steep slopes of the model layers, however, a 2-D numerical diffusion along model layers will imply a large but unwanted vertical mixing (e.g. between mountain tops and narrow valleys), especially in an atmosphere with strong stratification of the thermodynamic variables. To tackle this problem, a simple orographic flux-limiter is proposed which reduces numerical diffusion with increasing steepness of the topography.

The formulation of a monotonic scheme for horizontal numerical diffusion in the LM is based on the work of Xue (2000), who proposed two types of schemes: one based on Zalesak-type flux-correction (Zalesak, 1979) using the combination of high- and low-order schemes, and the other based on a simple flux-limiter which ensures that the diffusive fluxes are downgradient. The latter formulation, however, was found to be not strictly monotonic when applied to real cases. Thus, a third scheme is formulated which is based on direct multi-dimensional flux-limiting.

Section 2 summarizes the basic features of high-order numerical diffusion, followed by a description of three monotonic schemes in Section 3. The application of these schemes to simple 1-D and 2-D square wave tests is described in Section 4. In Section 5, an additional flux-limiter related to the slope of the model layers is introduced. The application of the new scheme to simulation of real cases with the LM is discussed in Section 6, and results from parallel test suites at MeteoSwiss and at DWD are described in Section 7. Finally, an outline of the technical implementation is given in Section 8.

2. High-Order Numerical Smoothing

Computational diffusion is mostly realized by introducing an additional operator to the right hand side of the prognostic equations:

$$\frac{\partial \psi}{\partial t} = S(\psi) + (-1)^{m/2+1} \alpha_m \nabla^m \psi \,, \tag{1}$$

where ψ is one of the prognostic variables and S represents all physical and dynamical source terms for ψ. The last term in Eq.(1) is the added linear diffusion term where m ($m = 2, 4, 6, \cdots$) denotes the (even) order of computational diffusion and α_m is the corresponding diffusion coefficient of order m.

The higher the order of the diffusion operator, the more scale selectively wavelength components are damped. Figure 1 shows the amplification factor (here: damping factor) for a one dimensional version of Eq.(1) using a forward in time and centred in space finite difference scheme for integration, plotted against the normalized wavelength $k\Delta x$ where k is the wavenumber and Δx is the grid spacing. For each of the second, fourth and sixth order schemes the corresponding diffusion coefficient α_m is chosen so that the shortest waves representable on a discrete grid ($2\Delta x$, i.e. $k\Delta x = \pi$) are damped completely within one integration time step.

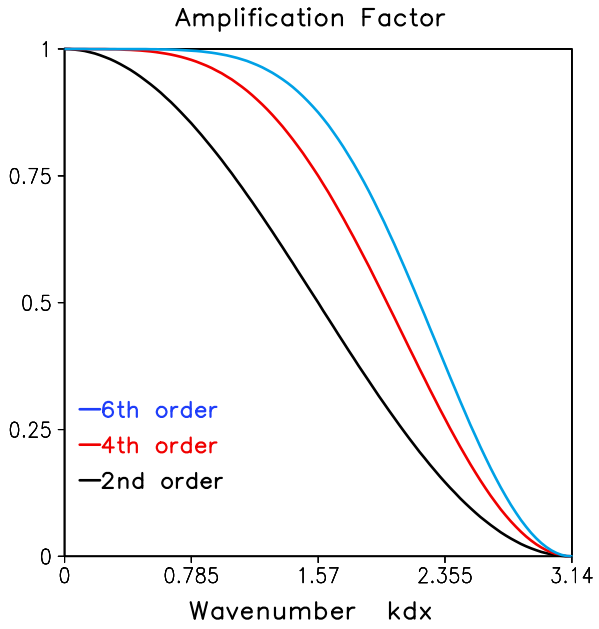

Figure 1: Amplification factor plotted against the normalized wavenumber

As can be seen from Fig. 1, all schemes damp not only the two grid interval wavelength, but also longer wave components in a wave spectrum. For example, the amplitude of a $4\Delta x$

wave is reduced by a factor of 0.5 in the second order scheme, and longer waves are also damped significantly. The fourth and sixth order scheme have much less damping for these longer waves, which contain physical meaningful information in a simulation and should not be affected by a numerical filter. Clearly, higher order schemes provide a more scale selective damping.

Many models use the 4th order linear computational diffusion scheme because of its relative computational efficiency compared to the 6th order scheme and of its superior damping properties compared to the second order scheme. Schemes of higher than 2nd order, however, have unwanted side effects. The 2nd order scheme has a Laplacian form and thus is always monotonic: by transferring higher values of the field into regions with smaller values no new minima or maxima can be created. This is not the case for the 4th, 6th and even higher order schemes, where spatial oscillations are introduced (Gibbs phenomenon), as can be seen in Fig. 2.

Figure 2 shows the one dimensional numerical solution of Eq.(1) (with $S = 0$) for 2nd, 4th and 6th order diffusion applied to an initial rectangular structure. The second order scheme (left) is strongly diffusive even for the large scale structure. At the end of the integration ($t = 100$) the amplitude of the entire square wave is significantly reduced. The 4th (middle) and 6th order (right) schemes retain the initial structure much better, and at the lateral edges, where short wavelengths components dominate, the sharp gradients are maintained in the solution (somewhat better by using the 6th order scheme).

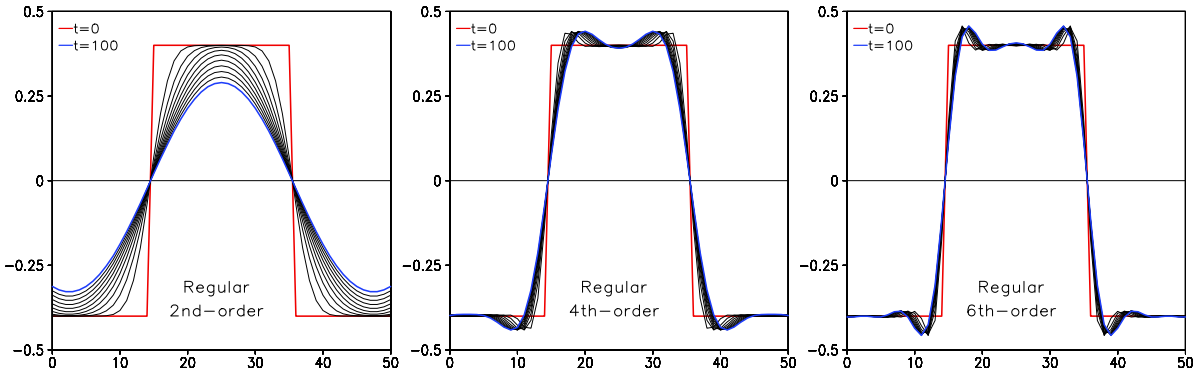

Figure 2: 1-D numerical solution of Eq.(1) for an initial square wave (red, $t = 0$) in case of 2nd (left), 4th (middle) and 6th order (right) linear diffusion. The domain has 51 grid points with a grid spacing of 1/50 m and the time step is 1 sec. The diffusion coefficients are chosen such that there is full damping of a $2\Delta x$ wave within one time step, i.e. $\alpha_m = (\Delta x/2)^m/\Delta t$. The solutions are plotted at 10 timestep intervals (thin lines).

However, over- and undershoots are generated by the numerical solution. The amplitude of these unphysical, both positive and negative spatial oscillations is increased by increasing the order of the diffusion operator. That is, going to higher than 4th order diffusion will not cure this side effect. Obviously, the $2\Delta x$ waves are removed from the solution, but at the cost of *introducing new noise on the resolvable scales*. In the context of a full simulation model these oscillations will interact nonlinearly with the physics as well as with the dynamics (as they are on the resolvable scales) and thus can result in unforeseeable effects. Moreover, negative oscillations are unacceptable for positive definite fields such as cloud water content or specific humidity.

3. Monotonic Diffusion Operators

This section describes three types of monotonic diffusion schemes. The first one is based on a Zalesak-type flux correction, similar to that used in many advection schemes. The second scheme is based on a simple flux limiter proposed by M. Xue (2000). And the third scheme uses a multidimensional flux limiter, where the formulation of the limiter factor closely follows the approach of Smolarkiewicz (1989).

The basic pre-requisite to apply these schemes is to rewrite the diffusion operator in Eq.(1) in a flux form. Omitting the source term S, the diffusive tendency then reads

$$\frac{\partial \psi}{\partial t} = (-1)^{m/2+1} \alpha_m \nabla^m \psi = -\nabla \cdot \mathbf{F}\,, \tag{2}$$

where $\mathbf{F}$ denotes the diffusive flux being defined by

$$\mathbf{F} \equiv (-1)^{m/2} \alpha_m \nabla (\nabla^{m-2} \psi)\,. \tag{3}$$

(a) Zalesak-type Flux Correction

Using the notations from Eqs.(2) and (3), the numerical scheme to integrate the 1-D version of the diffusion equation (the extension to more than one dimension is readily adopted) for a forward in time and centred in space scheme reads

$$\psi_i^{n+1} \;=\; \psi_i^n - (A_{i+1/2}^n - A_{i-1/2}^n), \tag{4}$$

where n denotes the time level, i is the gridpoint index and

$$A_{i+1/2}^n \equiv F_{i+1/2}^n \Delta t / \Delta x \tag{5}$$

denotes the normalized diffusive flux. Following the flux correction idea of Zalesak (1979), that was applied to the advection equation, Xue proposed a flux corrected scheme based on the combination of a low-order and a high-order diffusion scheme. Let A^L be the low-order diffusive flux, which is chosen to be of second order and thus will guarantee monotonicity, and A^H be a higher order diffusive flux, e.g. 4th or 6th order. Denoting the difference between the high-order diffusive flux A^H and the 2nd order one by

$$A^{HL} \;=\; A^H - A^L\,, \tag{6}$$

the Zalesak-type time integration scheme (4) can be written as

$$\begin{aligned} \psi_i^* &= \psi_i^n - (A_{i+1/2}^L - A_{i-1/2}^L)\,, \\ \psi_i^{n+1} &= \psi_i^* - (C_{i+1/2} A_{i+1/2}^{HL} - C_{i-1/2} A_{i-1/2}^{HL})\,. \end{aligned} \tag{7}$$

The factor C is called the flux correction coefficient or flux limiter, where $0 \leq C \leq 1$. When $C = 0$, the integration scheme (7) reduces to the 2nd order scheme, and when $C = 1$ it becomes purely high order. The idea is to use the high order scheme to the maximum extend possible, i.e. to reduce the fluxes by a factor C (to be determined for each grid interval interface) only when the monotonicity constraint is not met. As has been pointed out by Xue, the diffusion coefficients α_m of the low- and high-order schemes in the two step scheme (7) have to be chosen to be consistent with each other. To do so, it is required that two grid interval waves are damped by the same amount per time step. This means that different diffusion coefficients have to be used in the high-order flux A_H and in the low-order flux A_L. Longer waves, however, will be damped by a different amount.

Since the diffusion process should not generate new minima or maxima by stepping from the current time level n to the future time level $n+1$, the monotonicity constraint is chosen to be

$$\psi_i^{min} \leq \psi_i^{n+1} \leq \psi_i^{max}, \tag{8}$$

where ψ_i^{min} and ψ_i^{max} are the minimum and the maximum of ψ at the gridpoint and the adjacent points at the current time level n:

$$\psi_i^{min} = \min\left(\psi_{i-1}^n, \psi_i^n, \psi_{i+1}^n\right), \quad \psi_i^{max} = \max\left(\psi_{i-1}^n, \psi_i^n, \psi_{i+1}^n\right). \tag{9}$$

Following Zalesak, a flux limiter satisfying condition (8) can be defined as

$$C_{i+1/2} = \begin{cases} \min\left(1, R_{i+1}^+, R_i^-\right) & \text{if} \quad A_{i+1/2}^{HL} \geq 0\,, \\ \min\left(1, R_i^+, R_{i+1}^-\right) & \text{if} \quad A_{i+1/2}^{HL} < 0\,, \end{cases} \tag{10}$$

where

$$\begin{aligned} R_i^+ &= (\psi_i^{max} - \psi_i^*)/(A_i^{in} + \epsilon)\,, \\ R_i^- &= (\psi_i^{min} - \psi_i^*)/(A_i^{out} + \epsilon)\,. \end{aligned} \tag{11}$$

Here, ϵ is a small positive number to avoid division by zero. A_i^{in} and A_i^{out} are, respectively, the sum of all incoming and outgoing corrective fluxes A^{HL} of a grid box.

(b) The Xue Flux-Limiter

The monotonic scheme described above guarantees monotonicity, the computational costs, however, appear to be quite high. Xue pointed out that diffusive fluxes in high order schemes are not necessarily downgradient (as they are in the monotonic second order scheme) because they are no longer related to the local gradient of the diffused variable ψ. Upgradient fluxes can result in unphysical solutions and explain the over- and undershoots when applying high order schemes.

As a simple way to prevent upgradient fluxes to occur, Xue proposed to set the diffusive fluxes to zero whenever they have the same sign as the gradient of ψ. In the time integration scheme (4), the normalized fluxes A are thus replaced by

$$\tilde{A}_{i+1/2} = -A_{i+1/2} \min[0, \mathrm{sign}(A_{i+1/2}\delta_x\psi)]\,, \tag{12}$$

where the sign-function returns the sign of the argument. The application of this simple flux limiter in higher order diffusion schemes seems to prevent over- and undershoots in simple test cases. Obviously, the Xue-limiter (12) is far more efficient than the Zalesak-type flux corrected scheme since the extra computational costs are very small.

However, it cannot be shown analytically that the limiter will ensure strict monotonicity of the solution. Tests of the simple flux limiter (12) for the 4th order diffusion of real field distributions of cloud water and specific humidity have shown that over- and undershoots may still be present (see Section 4).

(c) Multidimensional Flux-Limiter

The multidimensional flux limiting scheme follows closely the ideas of the Zalesak-type flux correction scheme described above, but uses a direct limiter instead of the correction method based on antidiffusive fluxes. In this way, the two-step time integration scheme (7) as well as the problem of using consistent diffusion coefficients for low- and high-order fluxes is avoided. The construction of the limiter follows the approach of Smolarkiewicz (1989).

The numerical scheme for integrating the 2-D version of the diffusion equation using a forward in time and centred in space scheme reads

$$\psi_{i,j}^{n+1} \;=\; \psi_{i,j}^{n} - (A_{i+1/2,j}^{n} - A_{i-1/2,j}^{n} + A_{i,j+1/2}^{n} - A_{i,j-1/2}^{n}), \tag{13}$$

where n denotes the time level, (i,j) are the gridpoint indices with i counting in x-direction and j in y-direction, and

$$A_{\cdot,\cdot}^{n} \equiv F_{\cdot,\cdot}^{n} \Delta t/\Delta x \tag{14}$$

are the normalized $(m-1)$-th order diffusive fluxes at cell interfaces calculated from Eq. (3). The numerical scheme (14) can be rewritten as

$$\psi_{i,j}^{n+1} \;=\; \psi_{i,j}^{n} + A_{i,j}^{in} - A_{i,j}^{out}, \tag{15}$$

with $A_{i,j}^{in}$ denoting the sum of all fluxes into a grid cell and $A_{i,j}^{out}$ denoting the sum of all fluxes going out of a grid cell. Both the sum of the incoming and outgoing fluxes, $A_{i,j}^{in}$ and $A_{i,j}^{out}$, respectively, are defined to be positive. Using the notation

$$A_{\cdot,\cdot}^{+} = \max\left(A_{\cdot,\cdot}^{n}\,,\,0\right), \quad A_{\cdot,\cdot}^{-} = \min\left(A_{\cdot,\cdot}^{n}\,,\,0\right) \tag{16}$$

to indicate positive and negative fluxes at the cell interfaces, the sum of the incoming and outgoing fluxes is given by

$$\begin{aligned} A_{i,j}^{in} &= -A_{i+1/2,j}^{-} + A_{i-1/2,j}^{+} - A_{i,j+1/2}^{-} + A_{i,j-1/2}^{+}\,, \\ A_{i,j}^{out} &= +A_{i+1/2,j}^{+} - A_{i-1/2,j}^{-} + A_{i,j+1/2}^{+} - A_{i,j-1/2}^{-}\,. \end{aligned}$$

The difference $A_{i,j}^{in} - A_{i,j}^{out}$ is equivalent to the discretized total flux divergence. Since a monotonic numerical scheme shall not produce new minima or maxima within a time step, the monotonicity constraint is

$$\psi_{i,j}^{min} \;\le\; \psi_{i,j}^{n+1} \;\le\; \psi_{i,j}^{max}\,, \tag{17}$$

where $\psi_{i,j}^{min}$ is the minimum and $\psi_{i,j}^{max}$ is the maximum of the field variable ψ at the point (i,j) and the adjacent grid points at time level n:

$$\begin{aligned} \psi_{i,j}^{min} &= \min\left(\psi_{i,j}^{n}, \psi_{i+1,j}^{n}, \psi_{i-1,j}^{n}, \psi_{i,j+1}^{n}, \psi_{i,j-1}^{n}\right), \\ \psi_{i,j}^{max} &= \max\left(\psi_{i,j}^{n}, \psi_{i+1,j}^{n}, \psi_{i-1,j}^{n}, \psi_{i,j+1}^{n}, \psi_{i,j-1}^{n}\right). \end{aligned}$$

Using the monotonicity constraint (17) in the numerical scheme (15) yields

$$\psi_{i,j}^{min} \;\le\; \psi_{i,j}^{n} + A_{i,j}^{in} - A_{i,j}^{out} \;\le\; \psi_{i,j}^{max}\,. \tag{18}$$

Thus, the following conditions on the sum of the incoming and outgoing fluxes are sufficient to ensure monotonicity:

$$\begin{aligned} A_{i,j}^{in} &\le \psi_{i,j}^{max} - \psi_{i,j}^{n}\,, \\ A_{i,j}^{out} &\le \psi_{i,j}^{n} - \psi_{i,j}^{min}\,. \end{aligned}$$

With these conditions, the sum of all incoming fluxes cannot add more mass within one time step than that required to reach the maximum value $\psi_{i,j}^{max}$ and the sum of all outgoing fluxes cannot remove more mass than that to fall to the minimum value $\psi_{i,j}^{min}$. These conditions can be rewritten in the form of flux limiter ratios

$$\begin{aligned} \beta_{i,j}^{in} &= \frac{\psi_{i,j}^{max} - \psi_{i,j}^{n}}{A_{i,j}^{in} + \epsilon} \\ \beta_{i,j}^{out} &= \frac{\psi_{i,j}^{n} - \psi_{i,j}^{min}}{A_{i,j}^{out} + \epsilon}\,, \end{aligned} \tag{19}$$

where ϵ is a small number to avoid division by zero in the computer program. Whenever $\beta^{in}_{i,j} \geq 1$, the total incoming flux does not need to be modified. But if $\beta^{in}_{i,j} < 1$ the incoming fluxes are overestimated and the flux limiter has to be applied. Similar, if $\beta^{out}_{i,j} \geq 1$, the total outgoing fluxes will ensure monotonicity, but if $\beta^{out}_{i,j} < 1$, the outgoing fluxes are overestimated and have to be limited.

Since the total incoming and outgoing fluxes are additively composed of the fluxes at the cell interfaces, the limiter (19) is applied for each of these fluxes. And as the limiter for the incoming fluxes has been constructed independently of the limiter for the outgoing fluxes and because the outgoing flux at a cell interface is equivalent to the incoming flux at the adjacent cell, it is sufficient to simply take the minimum of both limiters. The application of the limiters (19) to the fluxes at the cell interfaces in the i- and j-direction can be written in a compact manner:

$$\begin{aligned} \tilde{A}^n_{i+1/2,j} &= \min\left(1, \beta^{out}_{i,j}, \beta^{in}_{i+1,j}\right) A^+_{i+1/2,j} + \min\left(1, \beta^{out}_{i+1,j}, \beta^{in}_{i,j}\right) A^-_{i+1/2,j}\,, \\ \tilde{A}^n_{i,j+1/2} &= \min\left(1, \beta^{out}_{i,j}, \beta^{in}_{i,j+1}\right) A^+_{i,j+1/2} + \min\left(1, \beta^{out}_{i,j+1}, \beta^{in}_{i,j}\right) A^-_{i,j+1/2}\,. \end{aligned} \tag{20}$$

For example, if the flux $A_{i+1/2,j}$ at the cell interface separating cell (i,j) and $(i+1,j)$ is positive, i.e. is an outgoing flux from cell (i,j) and thus an incoming flux for cell $(i+1,j)$, it will be limited with the minimum of the limiter $\beta^{out}_{i,j}$ of cell (i,j) and the limiter $\beta^{in}_{i+1,j}$ from cell $(i+1,j)$. By replacing the normalized fluxed A in the time integration scheme (13) with the limited normalized fluxes $\tilde{A}$ from Eq. (20), a monotonic diffusion scheme is finally obtained.

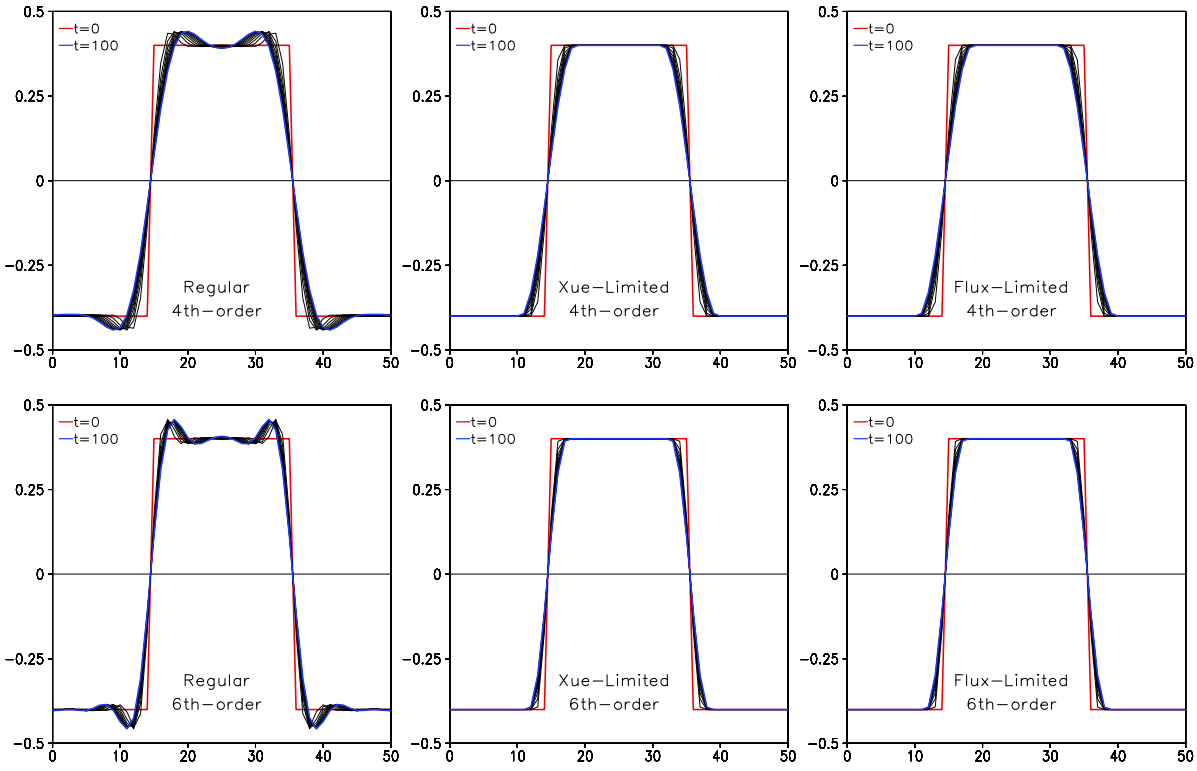

Figure 3: As in Fig. 2, but for 4th (upper panel) and 6th order (lower panel) linear diffusion. Left: Regular diffusion. Middle: Xue-limited diffusion. Right: Flux-limited diffusion.

4. Results from Simple Tests Cases

The solutions of the one-dimensional square waves test using 4th and 6th order regular diffusion as well as the monotonic scheme based on the Xue flux-limiter (12) and the scheme (20) based on direct flux limiting are shown in Figure 3.

Obviously, the unwanted numerical effects associated with the Gibbs phenomena are no longer present when using the simple Xue-limiter or the full flux limiter, but the smoothing characteristic is maintained in both schemes. The solution obtained with the Zalesak-type flux correction method (not shown) are very similar.

The extension of the monotonic schemes described in Section 3 to more than one dimension is straightforward. Fig. 4 shows the field distribution at initial time and the numerical solution obtained with 2nd-order diffusion after 100 time steps for the 2-D square wave test, where initially a block of 20 by 20 gridlines with a field value of 0.4 is placed in a background field having a value of -0.4. All parameters are the same as in the 1-D test, except that the diffusion coefficient for maximal damping has been adopted for the twodimensional case. Similar to the 1-D case, the initial distribution is significantly smoothed even at the larger scales. The peak value of 0.4 is reduced to 0.28 and the initial rectangular structure is no longer visible.

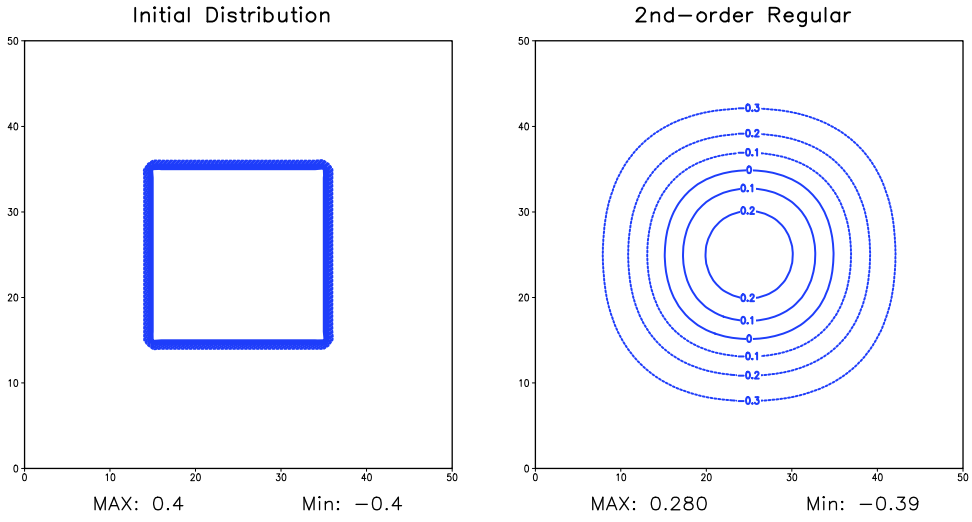

Figure 4: Contour maps of a field for the 2D square wave test. Left: Initial field distribution, where a block with field values with 0.4 is placed in a background field having the value of -0.4. Right: Solution of the 2nd-order regular diffusion after 100 time steps. The contour interval is 0.1

The results of the 4th-order regular linear diffusion and of the three alternative monotonic 4th-order schemes from Section 3 are shown in Fig. 5. When compared to the 2nd-order scheme, much sharper gradients at the lateral sides are retained by using the regular 4th-order diffusion scheme. Also, the large scale features of the initial field distribution are still visible. However, the 4th-order scheme suffers significantly from the Gibbs phenomenon, with severe overshoots of the order of 10% and undershoots of the order of 5% of the initial amplitude.

This effect is completely avoided by applying the Zalesak flux-correction scheme, the Xue-limiter or the multidimensional flux limiter. In all three schemes no over- or undershooting exists and the maxima and minima values of the field are exactly 0.4 and -0.4, respectively. Also, a slightly better gradient is maintained by the monotonic schemes compared to the solution from the regular 4th-order scheme and the rectangular shape of the contour lines

is retained somewhat better. The noisy appearance of the 0.4 and -0.4 contour line in the solution by the Zalesak scheme is due to roundoff errors which, however, have no detrimental impact.

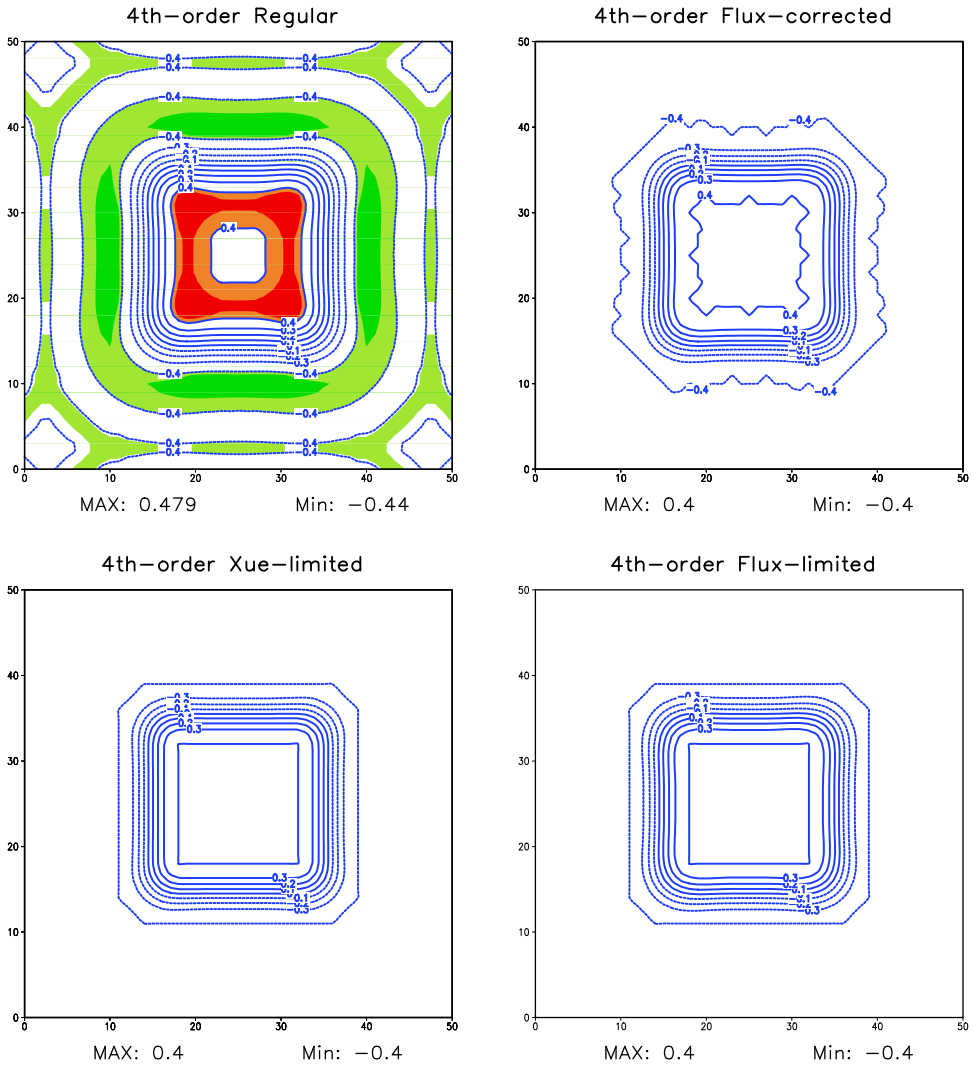

Figure 5: 2-D numerical solution of Eq.(1) for the square wave test after 100 time steps. Top left: 4th-order regular diffusion. Top right: 4th-order flux corrected. Bottom left: 4th-order Xue-limiter. Bottom right: 4th-order flux limited. Red shading indicates regions of overshoots, green shading regions of undershoots. The contour interval is 0.1.

All three schemes with monotonic limiters give very similar numerical solutions, but the simple Xue-limiter is the most efficient one as the additional computational costs are very small. Compared to the regular 4th-order diffusion, the computation time ratio of the Zalesak flux-correction scheme is 3.6, of the multidimensional flux-limiting scheme is 3.1, but is only 1.9 for the simple Xue-limiter (on an SGI Octane workstation).

Thus, from a practical point of view, the Xue-limiter seems to be the most efficient scheme to ensure monotonicity of high-order numerical diffusion. When applied to the cloud water field (a field with values varying within a few orders of magnitude) in simulations of real cases with the LM, however, this limiter was found to be not strictly monotonic. At a large number of gridpoints with a positive definite field distribution at the beginning of a time step, negative field values are observed after subjecting to 4th order diffusion with the Xue-limiter. To demonstrate this, a few gridpoint values (normalized by a factor) of a real

case simulation are chosen as initial condition for a 1-D numerical solution of the diffusion equation over 10 timesteps. In the beginning, a high value of water content is prescribed, with two much smaller side-maxima to the left and right, but separated by a zero value (see Fig.6). Structures like this are not too frequent but not unusual in simulations of real cases.

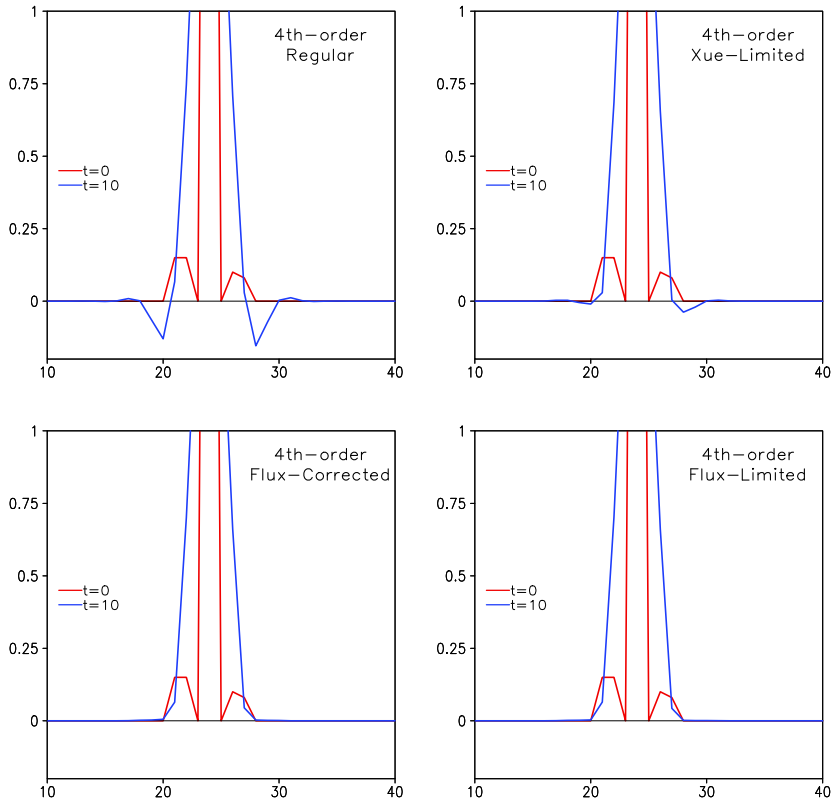

Figure 6: As in Fig. 2, but for a non-regular initial distribution (t=0, red) after 10 time steps (t=10, blue) for 4th-order diffusion. Top left: Regular. Top right: Xue-limiter. Bottom left: Flux-correction. Bottom right: Flux-limiting. The peak value of the initial distribution is 6.0.

The results of applying 4th-order numerical diffusion to this initial distribution using the regular scheme, the Xue-limiter, the Zalesak-limiter and the flux-limiter are shown in Fig. (6). Quite large undershoots with negative cloud water contents are generated by the regular scheme. This characteristic effect is drastically reduced by using the Xue-limiter, but is not cured completely: small negative values are still present in the solution. Both the flux-corrected and the flux-limited schemes guarantee a smooth and strictly monotonic solution.

Thus, the simple Xue flux-limiter seems not to be suited for application to the specific humidity and the specific water variables in a numerical prediction model, since spurious negative values of these variables may still be generated. For such fields, the schemes based on flux-correction or on flux-limiting should be used, where the multidimensional flux limiter is a little bit in favor because of its slightly better computational efficiency and a simpler formulation. For fields being not positive definite, as e.g. the velocity components, the Xue limiter is a viable and efficient alternative.

5. An Orographic Flux Limiter

Most mesoscale NWP models use a terrain-following sigma-type vertical coordinate and numerical smoothing is realized as horizontal diffusion, i.e. along quasi-horizontal surfaces of constant vertical coordinate. Over complex terrain, this may lead to systematic numerical biases which are induced by horizontal diffusion, as an unwanted vertical mixing in physical space will be implied. Clearly, the impact of this type of numerical error will increase with increasing steepness of the topography and is thus more noticeable in models with very high resolution.

For instance, if horizontal diffusion is applied directly to temperature in the prognostic equation for temperature, the smoothing will tend to cool the valleys and to heat the mountain tops in any stratification where the temperature decreases with height. Similarly, in an atmosphere with decreasing specific humidity with height, horizontal diffusion will dry the valley and moisten the mountains, which can have an unwanted positive feedback to precipitation formation over mountain tops.

Various modifications have been proposed to reduce the spurious biases resulting from quasi-horizontal mixing. Most models use a so-called slope correction for horizontal smoothing in the temperature equation, where instead of the actual temperature the difference of temperature and a reference profile is diffused. In LM, we use the model base state for this purpose. Errors from unwanted vertical mixing are then zero when the actual vertical temperature gradient is identical to the gradient of the base-state profile. However, when the profiles deviate from each other, large error may still be introduced (e.g. in very stable or unstable stratification). Slope corrections for other variables are normally not used.

Another popular method is the use of "true" horizontal diffusion, i.e. along surfaces of constant height or constant pressure (e.g. Zängl, 2000). Here, the values of the diffused variables at the adjacent gridpoints are interpolated to the height or pressure level of each gridpoint before diffusion is applied. Since the gridpoints usually have different heights, however, the diffusive fluxes at the cell interfaces will differ for neighboring gridpoints. Thus, mass conservation cannot be guaranteed with such a scheme. One could also try to locally reduce the value of the diffusion coefficient depending on the steepness of the orography (a commonly used measure is the Laplacian of topographical height). But here again the diffusive fluxes at the cell interface between two neighboring gridpoints will be different and mass can be artificially generated or lost.

Numerical smoothing schemes which introduce uncontrollable sources or sinks in momentum, heat or water mass are problematic, especially in an operational NWP model. With the flux-limited scheme discussed in the preceding Section, we have the opportunity to reduce the topography-induced biases without violating mass conservation: One can simply reduce the diffusive fluxes at the cell interfaces, depending on the steepness of the model surfaces. As the scheme is in flux-form, mass will be conserved automatically. And if the fluxes are artificially reduced before the monotonic flux limiters are applied, the monotonicity of the diffused field will also be guaranteed.

Two variants of this methods have been tested. The first is a non-continuous formulation, where the diffusive fluxes are simply set to zero whenever the height difference between two neighboring grid points exceeds a threshold value. Defining this height differences at cell interfaces and denoting them by

$$\Delta h_{i+1/2,j} = |h_{i+1,j} - h_{i,j}|\,, \quad \Delta h_{i,j+1/2} = |h_{i,j+1} - h_{i,j}|\,, \tag{21}$$

where $h_{i,j}$ is the geometrical height of a grid point at a surface of constant vertical coordinate,

the limiter function for the diffusive fluxes A in Eq. (13) can be written as

$$A_{i+1/2,j} = \begin{cases} F_{i+1/2,j}\frac{\Delta t}{\Delta x}, & \text{if} \quad \Delta h_{i+1/2,j} \leq H_{max}\,, \\ 0\,, & \text{if} \quad \Delta h_{i+1/2,j} > H_{max}\,, \end{cases}$$
$$A_{i,j+1/2} = \begin{cases} F_{i,j+1/2}\frac{\Delta t}{\Delta x}, & \text{if} \quad \Delta h_{i,j+1/2} \leq H_{max}\,, \\ 0\,, & \text{if} \quad \Delta h_{i,j+1/2} > H_{max}\,. \end{cases} \tag{22}$$

Here, H_{max} is a threshold value for the maximal height difference. Another approach is to gradually reduce the fluxes with increasing steepness. One can try various functional dependences, but to keep things simple we apply a simple quadratic form, where the fluxes become zero when the threshold value for the height difference is exceeded:

$$A_{i+1/2,j} = \max\{\,0\,, 1 - (\Delta h_{i+1/2,j}/H_{max})^2\} \cdot F_{i+1/2,j}\frac{\Delta t}{\Delta x}\,.$$
$$A_{i,j+1/2} = \max\{\,0\,, 1 - (\Delta h_{i,j+1/2}/H_{max})^2\} \cdot F_{i,j+1/2}\frac{\Delta t}{\Delta x}\,. \tag{23}$$

Tests of the application of the orographic flux limiters (22) and (23) are discussed in Section 6.2.

6. Results from Test Simulations with the LM

This Section describes some results from single test simulations of real cases using the current operational version of LM (lm_f90, V 2.6). The basic model setup is identical to the operational configuration (7km grid spacing, 40 sec timestep, full physics). First, the impact of monotonicity is discussed in Section 6.1. Second, the application of the orographic flux-limiters is described in Section 6.2.

6.1 The Impact of Monotonic Flux-Limiting

As a first test, the Xue limiter was applied to all prognostic variables for a randomly chosen real case from 18 September 2000. Figure 7 shows the vertically integrated cloud water content of a 12h-forecast starting at 00 UTC. Concerning the structure of the two cloud bands over Denmark and over the Northern Sea, no apparent differences between the reference run using regular 4th order diffusion and the model version with monotonic diffusion can be noticed. However, the area mean value of the integrated cloud water content is slightly reduced from 41 to 38 gm^{-2}.

This can also be noticed from the scatter diagram (Figure 7, right), where the gridpoint values of the integrated cloud water content of the reference run (y-axis) are plotted against those from the experiment (x-axis). Obviously, the values obtained from the reference are on average somewhat larger than those resulting from the run with monotonic diffusion. The same type of impact can also be noticed in the precipitation amount, which is slightly smaller in the experiment (not shown). One could attribute this to the removal of overshoots from the solution for the cloud water field. In a complex nonlinear model, however, such a clear assignment of cause and effect is not possible. Due to the noticeable effect on the cloud water content, a more thorough evaluation is necessary to assess the impact of the monotonic diffusion scheme on the cloud-radiation interactions.

6.2 The Impact of Orographic Flux-Limiting

First test integrations using the monotonic flux limiter (20) in connection with the orographic limiter (23) have been performed for a number of cases from the period October-November 2000. During this time, a synoptic-scale weather situation with southerly flow over the Alps

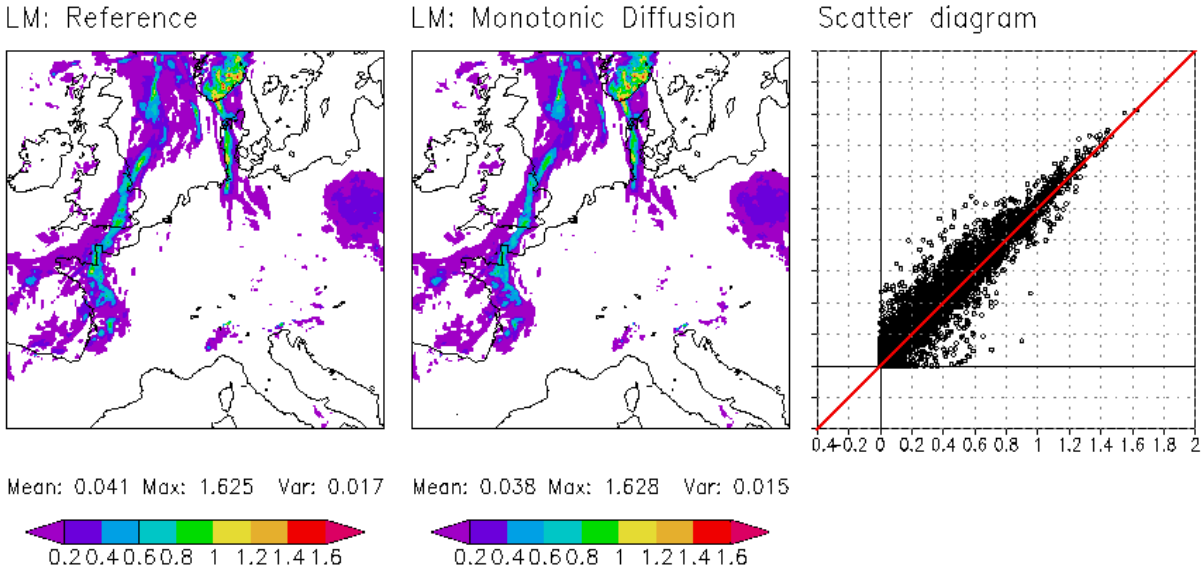

Figure 7: Vertically integrated cloud water (kg/m^2) content of a 12-h LM forecast starting at 18 September 2000 00 UTC. Left: reference solution with 4th oder regular diffusion; middle solution from a run with monotonic Xue limited diffusion; right: Scatter diagram of values from the reference (y-axis) viz. experiment (x-axis) runs.

prevailed, causing often a Föhn-effect in regions to the north of the Alps with blocking or weakening of cold fronts from the west. In the operational forecasts with the LM at DWD, however, the Föhn-effect was overestimated in most cases. This can be noticed when comparing the monthly mean precipitation from the forecasts and from a high resolution observation network for October 2000 in Fig. 8: The precipitation amount for southwestern Germany and for Bavaria is severely underpredicted due to a too frequent blocking or too strong weakening of fronts. A similar underprediction is noticed for the northern and western parts of Switzerland.

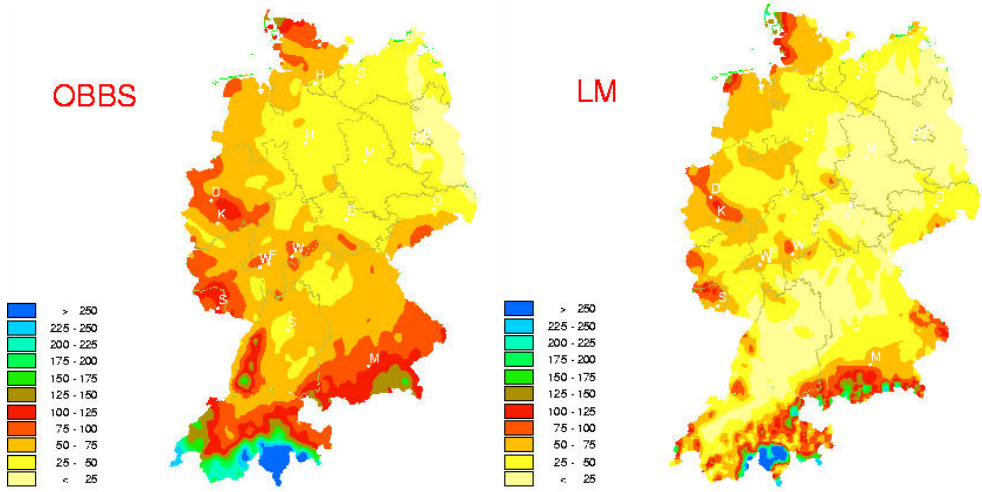

Figure 8: Monthly precipitation amount (mm) for October 2000 as observed (OBBS) by climate networks (max: 525 mm, mean: 63mm) and derived from 00 UTC LM forecasts (+30h - 06h) at DWD (max: 999 mm, mean: 69mm).

During a number of experimental studies related to the failure of the model forecasts for these Föhn situations, it was found that horizontal diffusion has an unexpected large dynamical

impact on the onset and strength of the Föhn flow. As an example, we choose here the forecast starting from 00 UTC at 11 October 2000. For experimentation, a somewhat smaller model domain (241x241 gridpoints) than the operational one (325x325 gridpoints) has been used. The initial and boundary conditions come from interpolated GME data.

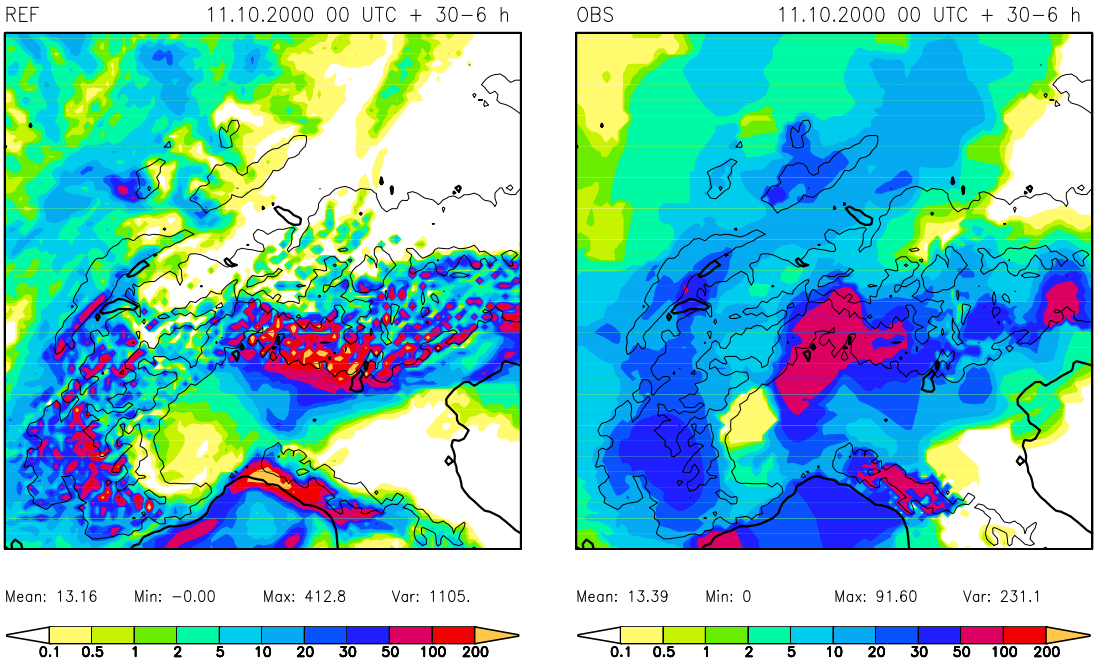

Figure 9: 24h accumulated precipitation (mm) for 11 October 2000 00 UTC +06h ...+30h. Left: Reference run. Right: Analysis based on Synop observation. The thick contour lines show the land-sea mask, the thin lines are the 700m and 2100m contour lines of orography

Fig. 9 compares the 24 h accumulated precipitation amount from the reference run (left) and from the Synop observations (right) on a model subdomain of about 700x700 km covering the Alpine region. As the observation come from the rather coarse SYNOP network, the structure of the precipitation field is only a first guess and many details may be lost. Nevertheless, the observation indicate a large region along the southern ridge of the Alps with precipitation amounts in the range 50 - 100 mm (which resulted in a severe flooding event in the Turin region). This is well captured by the model forecast, the centre is shifted somewhat to the east. The peak precipitation, however, is certainly overestimated by the model. Another region with high precipitation amounts is along the western ridge of the alps, but also here the peak values seem to be too high. In general, the forecasted precipitation field looks very noisy, with $2\Delta x$ structures located in regions of steep topography. This is not believed to be realistic.

The effect of a too strong blocking by southerly Föhn flow is obvious in the northern part of the Alps: whereas the observations indicate precipitation amounts in the range of 5 - 20 mm in a region extending from the Lake of Geneva over the Lake of Constance into the southwestern parts of Bavaria, the forecast gives almost no indication of precipitation at all, except for a spotty structure over northern Switzerland. Another typical feature of many LM precipitation forecasts can also be noticed: The valley of Valais, a steep valley extending southeast of the Lake of Geneva, remains almost dry, whereas a large amount of rain and snow falls over the mountain tops at the valley sides. The observations, however, indicate significant precipitation at the valley ground.

The impact of monotonic and orographic flux limiting for horizontal diffusion to the precipitation forecast is quite large. The left picture in Fig. 10 displays the result obtained with the quadratic form (23) of the orographic limiter with H_{max} set to 250 m. This limiter is only applied for temperature perturbation, specific humidity and cloud water content, whereas pressure perturbation and the wind components are treated with the computationally more efficient Xue limiter. Experiments have shown that the application of the flux-limiter scheme to the latter variables has not a significant impact to the forecasts. They are thus treated with the computationally more efficient Xue-scheme.

When compared to the reference run, the precipitation pattern looks less noisy than in the reference run and a part of the $2\Delta x$ structures are gone or their amplitude appears to be smaller: the field variance is reduced from 1105 mm down to 890 mm and the field maximum from 413 mm to 355 mm. Also, the southwest-northeast orientation of the small-scale precipitation bands over the western parts of the Alps has changed to a more northwest-southeast orientation. As a distinct feature of the new scheme, the "dry valley effect" seems to be cured: with flux-limited horizontal diffusion a significant precipitation amount is now predicted for the valley of Valais. Most interestingly, a coherent rainband extending from northern Switzerland to western Bavaria is now formed, with an eastern boundary close to the observed one. Clearly, a large part of precipitation is still missing to the west of this band, but this experiment indicates that a too strong horizontal diffusion over steep terrain can have significant effects to the fields far away.

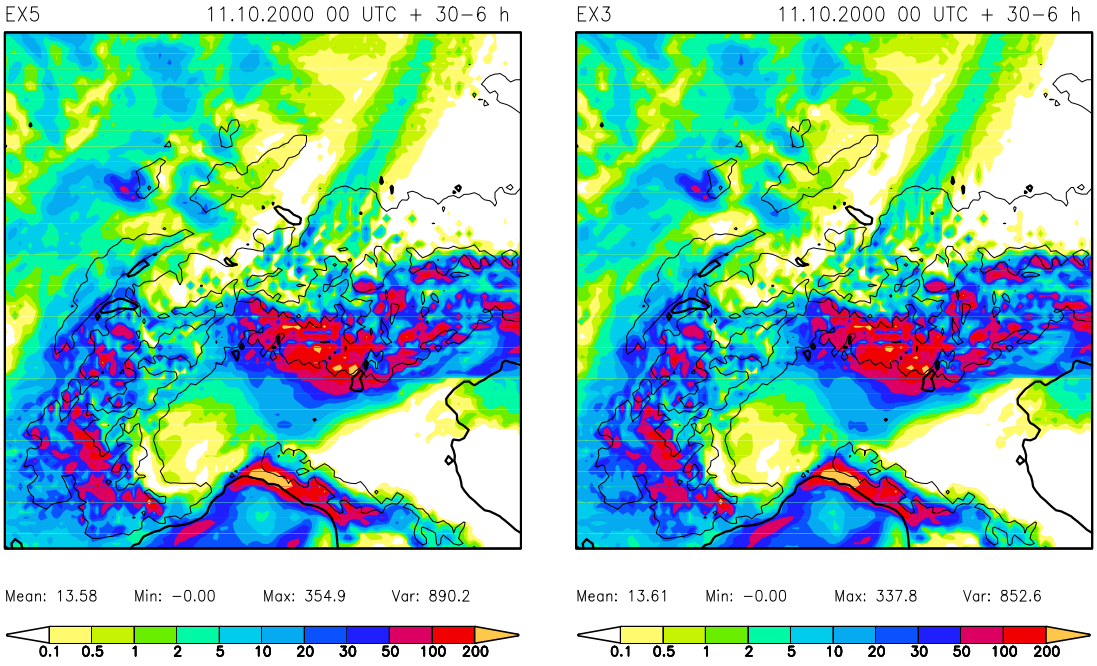

Figure 10: As in Fig. 9 but for the flux-limited diffusion scheme using the quadratic form (23) of the orographic flux limiter (left). Right: The same scheme, but with generally reduced diffusion coefficients for temperature and pressure perturbation (by a factor of 0.6) and for water vapour and cloud water (by a factor of 0.3).

Also, a number of test runs using generally reduced diffusion coefficients have been performed since overdamping over complex terrain was found to be crucial for the failure of the precipitation forecasts. The right picture in Fig. 10 shows the result from a run using a reduction factor of 0.6 and of 0.3 for the default diffusion coefficient for temperature and pressure perturbation and for water vapour and cloud water, respectively. There is not too much difference between the results, the run with reduced coefficients is slightly more smooth

and has a lower field maximum. This beneficial impact of smaller diffusion coefficients is lost with a further reduction, since a certain amount of damping is necessary to control small-scale noise. As a default for the reduction factors for the diffusion coefficients for heat and moistures, the values 0.75 and 0.5 have been implemented.

The stepwise form (22) of the orographic limiter behaves in general very similar to the continuous quadratic form (23). The latter version, however, gives a slightly more smooth solution and the extra computational costs are negligible. Thus, the limiter (23) was implemented. Additional sensitivity tests concerning the threshold value H_{max} for the maximum height difference between neighboring gridpoints in the limiter function (23) have been performed. For a very high value of H_{max} the results tend to become similar to the monotonic scheme using no orographic limiter, and for a very low value the scheme tends to produce an underdamped, i.e. very noisy solution. For values between 200 m and 300 m, the results are quite similar and thus $H_{max} = 250$ m has been implemented as a default. Clearly, this applies only for the current 7 km grid spacing, and a resonable value has to be set for other horizontal resolutions.

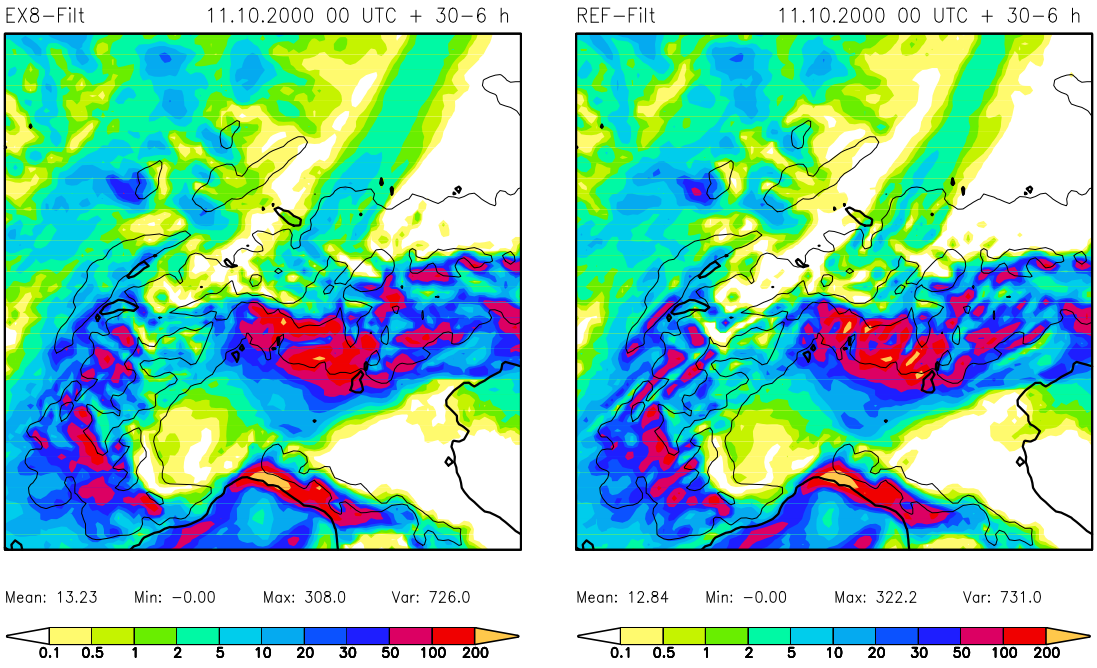

Figure 11: As in Fig. 9 but for the filtered topography. Left: Quadratic form (23) of the orographic flux limiter and with reduced diffusion coefficients for heat (factor 0.75) and moisture (factor 0.50) (left). Right: reference run.

All test runs described above have been done with the original mean topography at the grid scale. Using a mean topography, however, constantly forces the generation of $2\Delta x$-waves, which are represented hopelessly inaccurate in numerical models. Thus, a filtering of topography has been introduced in the operational applications of the LM in order to get a more correct interaction of dynamics with the surface. For this purpose, the Raymond (1988) filter is applied which removes $2\Delta x$ and $3\Delta x$ wave components from the mean orography (Gassmann, 2001).

Since the filtered orography is smoother and less steep, the errors from horizontal diffusion are expected to become smaller. And indeed, reruns of cases from the Föhn period during October-November 2000 showed a beneficial impact of topographical filtering to precipitation and 2m-temperature forecasts. The right hand picture in Fig. 11 displays the 24-h

precipitation amount for the 11 October case using the filtered topography and standard horizontal diffusion. When compared to the reference run using the mean topography (Fig. 9, left), the precipitation field has become much less noisy. Also, the blocking effect north of the Alps is reduced and a rainband in southern Germany appears. However, there is still a noticeable impact of using monotonic horizontal diffusion with the orographic limiter (Fig. 11, left): The rainband appears to be slightly broader and more intense, and the unrealistic southeast-northwest orientation of precipitation bands over the western part of the Alps is removed.

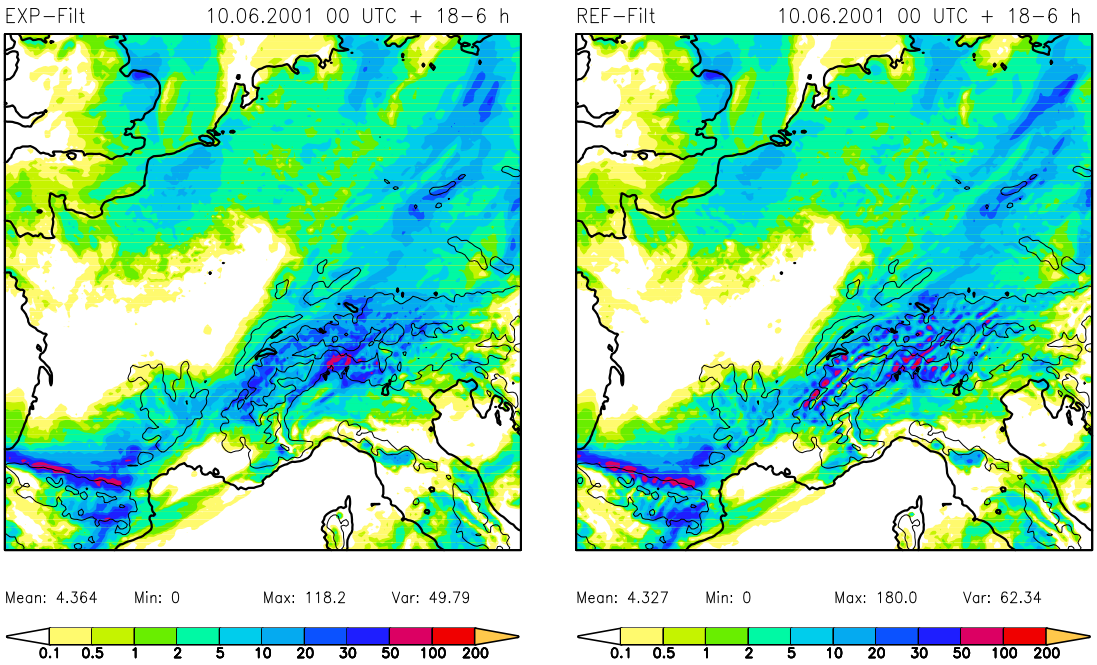

Figure 12: 24h accumulated precipitation (mm) for 10 June 2001 00 UTC +06h ...+18h. Left: Default version of the flux-limited scheme for horizontal diffusion. Right: Reference run. The thick contour lines show the land-sea mask, the thin lines are the 700m and 2100m contour lines of orography

The beneficial impact of the new diffusion scheme is noticeable also in cases other than Föhn flow. For instance, Fig. 12 compares the 12-h precipitation amount for 10 June 2001 as predicted with the standard scheme for horizontal diffusion (right) and with the default version of the flux-limited scheme (left), where in both runs the filtered topography is used. On this day, a frontal system moved slowly eastwards with only weak winds over the Alpine region. Most of the precipitation is stratiform since a stable thermodynamic stratification prevailed. In the reference run, the predicted precipitation is rather noisy with high peak values over the Alps and the Pyrenees. Also, there is an organization of the maxima along a southeast-northwest line in these areas, which is related to bands of positive and negative vertical velocity being formed perpendicular to the flow direction. These structures are not believed to be realistic but the mechanisms for their formation are not yet clear. In the run with the new diffusion scheme, the amplitude of these vertical velocity bands is strongly reduced, resulting in a much smoother precipitation field over the mountainous regions.

7. Results from Parallel Experiments

Tests experiments with the modified horizontal diffusion scheme have been conducted at MeteoSwiss and at DWD over longer time periods. At MeteoSwiss, the LM was rerun for November 2000 and compared with the operational implementation and with model versions

using topographical filtering. The stepwise form (22) of the orographic limiter was used. At DWD, the period from 31 July 2001 to 24 August 2001 was rerun using the continuous form (23) of the topographical limiter function. In this experiment, the full data assimilation cycle including the soil moisture analysis has been involved. Also, a weak filtering of topography is used as in the operational model version. For the impact of the filtering of LM-topography, see Gassmann (2001).

7.1 Parallel Runs at MeteoSwiss

The test experiment for November 2000 was evaluated using the standard Swiss verification package (F. Schubiger, pers. comm.) for surface parameters. The verification is against measurements taken by synoptical and automatic stations in Switzerland (the ANETZ).

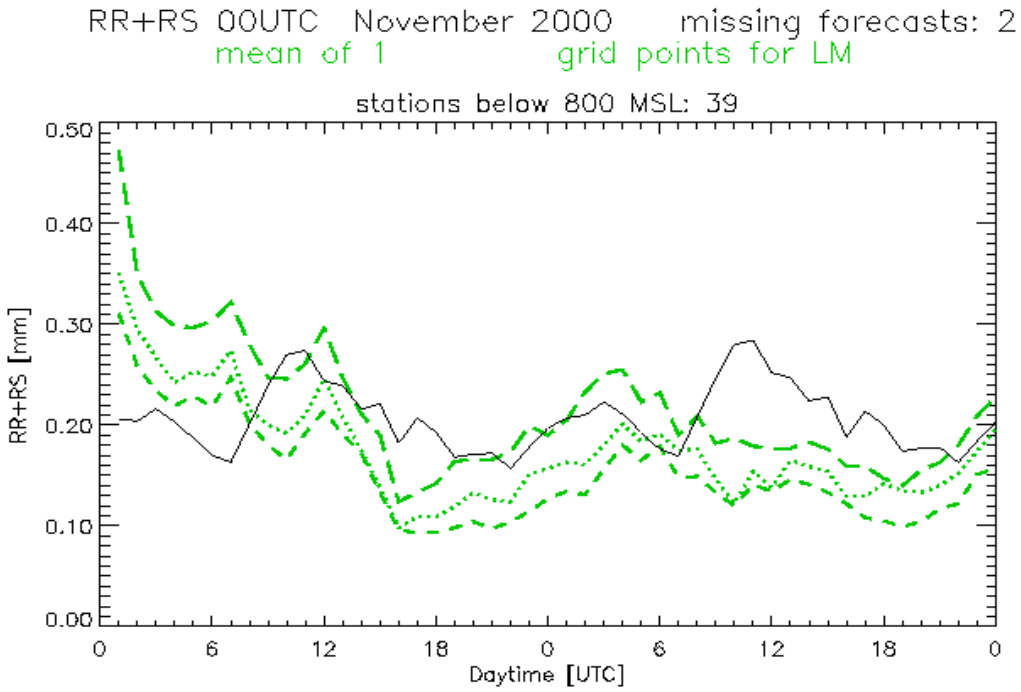

Figure 13: Monthly mean diurnal cycle of predicted and observed precipitation for November 2000 at ANETZ-stations in Switzerland. Full line: observations. Short-dashed line: model version with weak filtering of topography. Dotted line: model version with strong filtering of topography. Long-dashed line: model version with weak filtering and modified horizontal diffusion.

Figure (13) shows the monthly mean diurnal cycle of total precipitation for the 48-h forecast period of all 00 UTC runs compared to the observations. All three model versions overestimate the precipitation amount during the first 6 hours of simulation time because of the spin-up phenomenon (no data assimilation has been used). Later on, the forecasts using a weak topographical smoothing with a filter-parameter $\epsilon = 0.1$ underestimate the observed amount of rain and snow significantly, but less than the former operational version without filtering (not shown). A much stronger smoothing of the topography by using $\epsilon = 10.0$ results in slightly larger precipitation amounts which, however, are still below the level indicated by the observed data. The combination of the weakly filtered topography with the new scheme for horizontal diffusion fits more closely to the observations during most of the simulation time.

The verification shown in Fig. (13) used the nearest-gridpoint method, i.e. only one LM-gridpoint was used for the comparison with the observation. It is interesting to note that

the results depend on the method used for verification: If a horizontal average of 5 or 13 gridpoints is used (upscaling), then the predicted precipitation amounts for the model versions using a filtered orography increase slightly to compare more favorably with the observations. However, when the modified diffusion scheme is applied, then the results depend much less on the verification method. This indicates a much smaller spatial variability than when using a filtered topography only.

Table 1: Frequency bias of 00 UTC LM precipitation forecasts during November 2000 at ANETZ-stations in Switzerland (all 6-h intervals of 48hr forecasts).

Station Selection	Model Version	Threshold (mm/6h) at				
		0.1	2.0	10.0	30.0	50.0
Stations < 800 m	LM filt+hdiff	108	93	89	170	-
	LM at Met.Sw.	87	57	61	105	-
	LM at DWD	74	48	48	35	-
All stations	LM filt+hdiff	111	88	72	126	-
	LM at Met.Sw.	95	63	51	78	-
	LM at DWD	84	54	41	32	-

The frequency bias of the LM-forecasts for November 2000 at ANETZ-stations is shown in Table 1 for various threshold values, where all 6-h intervals of the 48-h forecasts have been considered. The upper part of the table gives the results for all stations with altitude below 800 m, i.e. mountain stations have been excluded. The operational LM-versions at MeteoSwiss and at DWD, which both were run without topographical filtering at that time, show a significant underestimation of precipitation, especially for precipitation amounts exceeding the 2mm/6h and 10mm/6h thresholds. This underestimation is more severe in the DWD model version (using a full data assimilation cycle). Note that the heavy precipitation class with a threshold of 30mm/6h is statistically not significant (only 0.3% of all cases) and thus is not considered here. By applying a weak topographical filtering and the new horizontal diffusion scheme (LM filt+hdiff), the higher precipitation amounts are much better represented in the model forecasts: there is still an underestimation, but it is much smaller than with the operational version. For smaller precipitation amounts with a threshold of 0.1 mm/6h, however, a slight overprediction can be noticed.

The impact of the new scheme for horizontal diffusion is much smaller for surface parameters other than precipitation. Figure (14) displays the mean diurnal cycle of 2m-temperature (top) and 2m-dewpoint depression (bottom) for November 2000 over Switzerland. The model version without filtering of topography underestimates the extrema of the 2m-temperature, but more severe the nighttime minimum, resulting in a too large amplitude of the 2m-temperature (5.7 K compared to the observed 3.6 K on day 2). The model version with filtered topography reduces this amplitude error by about 50 %, the amplitude is only 4.9 K in this case. An additional inclusion of the new horizontal diffusion scheme has only a slight impact with a further reduction of the amplitude to 4.7 K. The 2m-dewpoint depression appears to be too large in the standard model runs, i.e. the surface layer is too dry over the Alpine area. By using a filtered topography, this type of error is significantly reduced, especially during nighttime. At noon, the model is now simulating a slightly too moist surface layer. An additional moistening effect can be noticed from applying the new horizontal diffusion scheme.

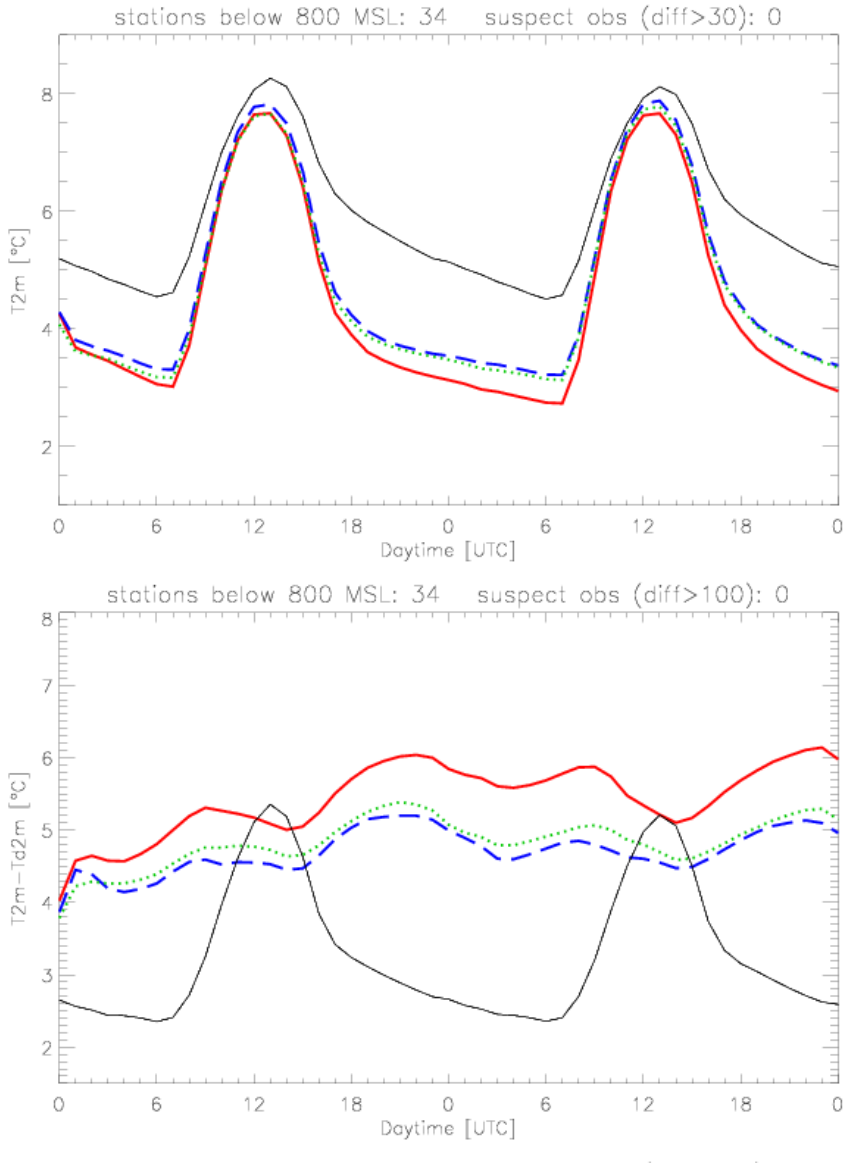

Figure 14: Monthly mean diurnal cycle of predicted and observed 2m-temperature (top) and 2m-dewpoint depression (bottom) for November 2000 at ANETZ-stations below 800m altitude in Switzerland. Full black line: observations. Full red line: former operational version without filtering of topography. Dotted green line: model version with weak filtering of topography. Dashed blue line: model version with weak filtering and modified horizontal diffusion.

7.2 Parallel Runs at DWD

The parallel test experiment at DWD for the August 2001 period was evaluated using the standard verification package for surface weather parameters (U. Damrath, pers. comm.). The verification is against observations from Synop Stations in the integration domain of LM at DWD, and the only difference between the operational and the experimental runs is the inclusion of the new horizontal diffusion scheme.

Fig. (15) shows mean verification scores of various surface parameters as a function of forecast time for all weather stations in the domain. The root mean square errors of 10m-wind, surface pressure, 2m-temperature and 2m-dewpoint depression, as well as the percent-correct score for cloud cover, are practically the same for the experimental and operational runs. A slight improvement with the new version of LM can be noticed for precipitation, especially for

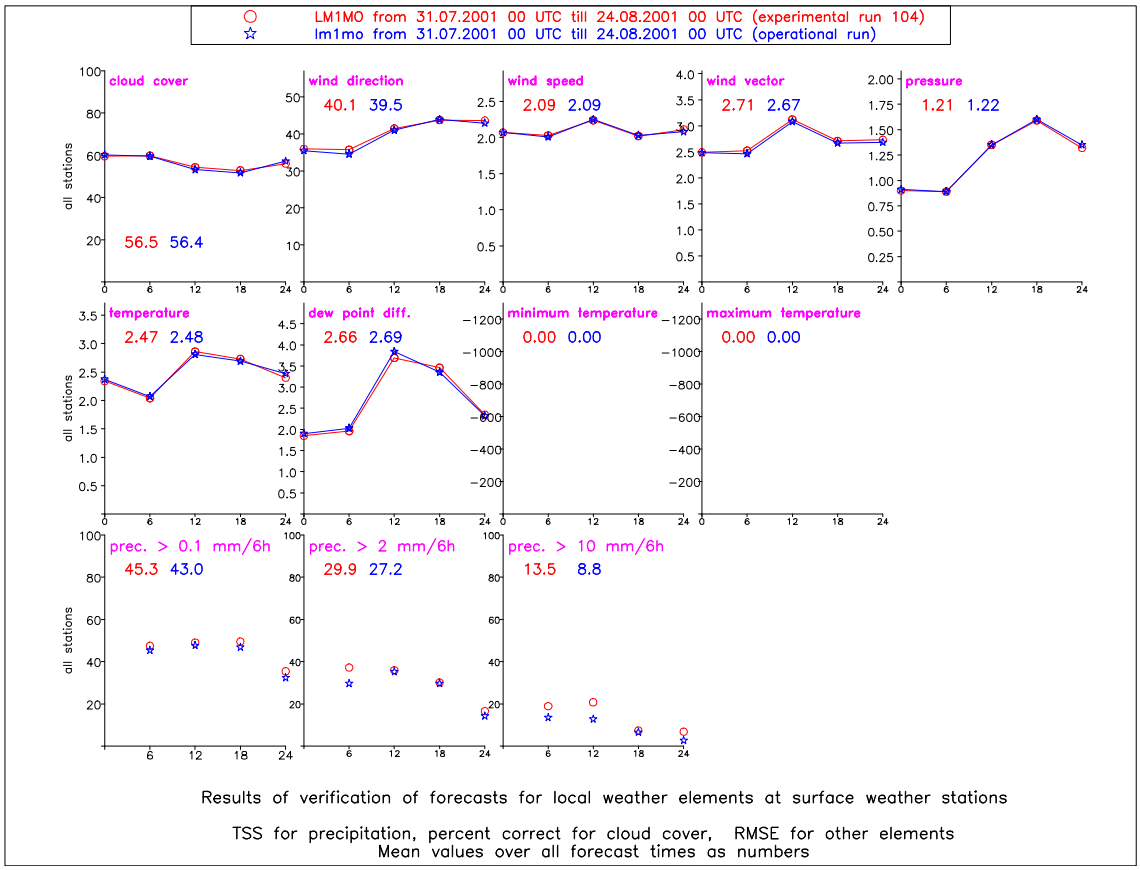

Figure 15: Mean verification scores at all Synop Stations in the LM integration domain for the period 31 July to 24 August 2001 as a function of forecast time (00, 06, 12, 18, 24 h). Verification time is 00 UTC. Red – experimental run exp_104, blue – operational run. Root-mean-square error for all elements except for cloud cover (percent correct) and precipitation (TSS); numbers are mean values over all forecast times. Top (from left to right): cloud cover, wind direction, wind speed, wind vector and surface pressure. Middle (from left to right): temperature, dew point difference, minimum and maximum temperature. Bottom: TSS of 6 h precipitation amounts (prec) for the three indicated threshold values.

higher precipitation amounts. For a threshold value of 10mm/6h the TSS score increases from 8.8 to 13.4, indicating a more reliable prediction of heavy precipitation events.

When considering mean verification scores of all stations in the domain, there will be a large contribution of stations in non-mountainous areas. Fig. (16) displays the mean verification scores for Synop Stations with an altitude between 300m and 800m above sea-level. These stations are representative for mountainous areas in the vicinity of steep terrain, where the impact of the orographical limiter in the diffusion scheme is expected to be more noticeable. As in case of all stations, the scores for the 10m-wind and surface pressure are indifferent to the change in the horizontal diffusion scheme. However, there is a marginal improvement of cloud cover, and the rmse-errors for the 2m-dewpoint depression are slightly smaller, whereas the rmse-errors of the 2m-temperature remain practically the same. This indicates – similar to the verification results in Fig. (14) for the diurnal cycle of 2m-temperature and dewpoint over Switzerland – that the near-surface moisture is affected by the orographically limited diffusion to a larger extend than temperature. The quality of the precipitation forecasts increases significantly for all threshold values, as seen in the lower panel of Fig. (16).

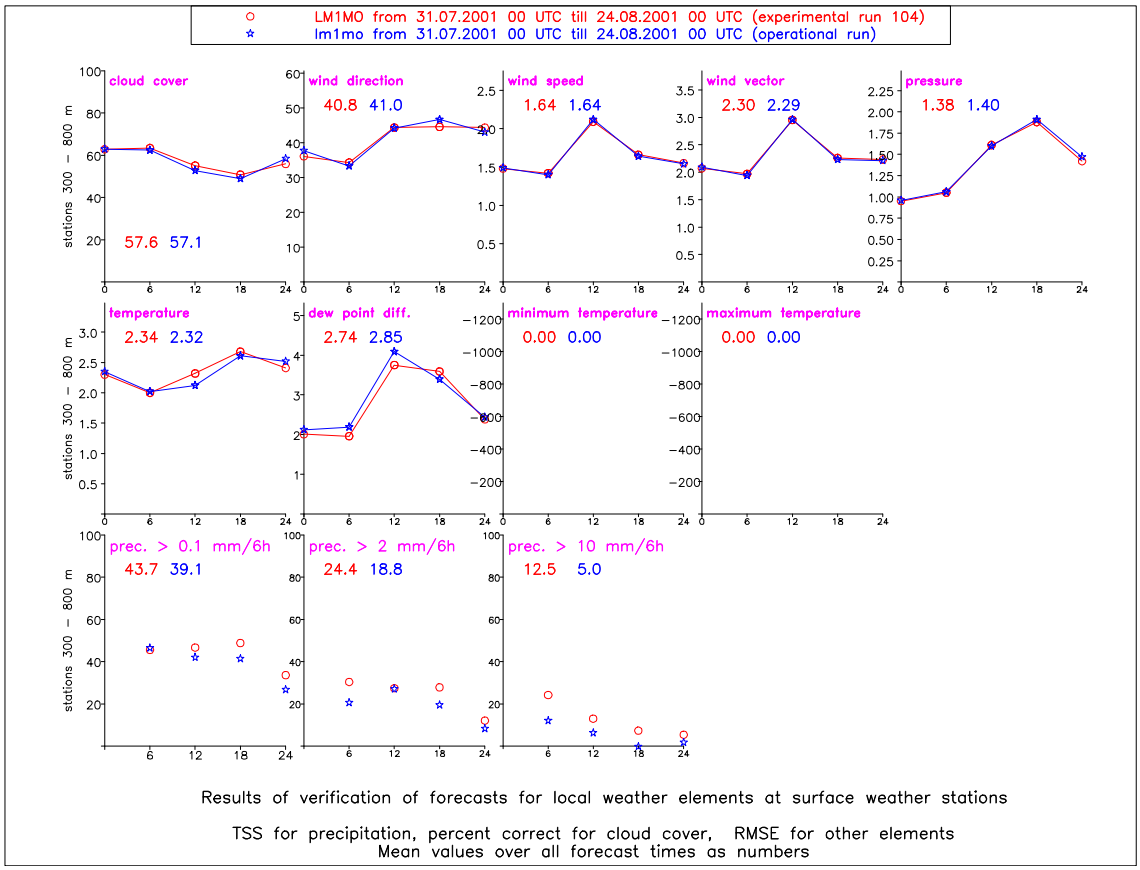

Figure 16: As in Figure 15 except for all Synop Stations with an altitude between 300m and 800m above sea-level.

8. Implementation of the Scheme

The new scheme for monotonic numerical diffusion including orographic flux limiting has been implemented as an option in model version `lm_f90 V 2.9`. It can be switched on by setting the parameter `itype_hdiff = 2` in the NAMELIST-Input list `INPUT_DYN`. Orographic limiting is done for temperature, specific humidity and specific cloud water content only. All other prognostic variables, i.e the three wind components and the perturbation pressure, are treated with the quasi-monotonic Xue limiter. Three additional control parameters have been introduced in this NAMELIST-Input group. Table 2 summarizes the new input parameters.

Table 2: New control parameters in the NAMELIST-Input group `INPUT_DYN`.

Parameter	Definition / Purpose	Default value
`itype_hdiff`	a switch to select a scheme for horizontal diffusion =1: regular 4th-order linear horizontal diffusion =2: new monotonic 4th-order scheme	`itype_hdiff = 2`
`hd_max:`	the threshold value H_{max} in the quadratic form (23) of the orographic flux limiter in m.	`hd_max = 250`
`hd_cor_t:`	a factor by which the standard coefficient for numerical diffusion is reduced in case of temperature and pressure smoothing.	`hd_cor_t = 0.75`
`hd_cor_q:`	a factor by which the standard coefficient for numerical diffusion is reduced in case of humidity and cloud water smoothing.	`hd_cor_q = 0.50`

9. Summary

Most NWP models require numerical smoothing to damp small-scale (2 grid interval) noise being related to stepwise or singular signals which are permanently generated in a nonlinear model. Regular high order linear diffusion, however, tends to introduce unphysical solutions and thus new noise on the resolvable scales. In order to achieve monotonic and mass-conserving numerical diffusion, a new scheme based on direct multi-dimensional flux-limiting has been constructed.

Tests with 1-D and 2-D idealized cases show the beneficial impact of the new scheme. All over- and undershoots are removed from the solution. In contrast to a simple version using the Xue-limiter, the scheme with a direct flux-limiter guarantees a strictly monotonic solution. In LM simulations of real cases considered so far, there is only a relatively small impact from using monotonic 4th order diffusion with a tendency for lower vertically integrated cloud water and smaller peak precipitation amounts.

Numerical smoothing is often realized as horizontal diffusion, i.e. along surfaces of constant vertical coordinate. As most NWP models use a terrain-following vertical coordinate, this will result in systematic numerical biases, as an unwanted vertical mixing in physical space is implied. This type of numerical error will increase with increasing steepness of the topography, and thus poses a severe problem in high-resolution regional models. Current remedies, such as doing diffusion on z- or p-surfaces or applying a local reduction of the diffusion coefficients, are not mass-conserving and will thus introduce other errors. With the new smoothing scheme, the topography-induced biases can be reduced without violating mass conservation while still maintaining monotonicity by simply applying an orographic limiter to the diffusive fluxes at cell interfaces.

LM test simulations with the orographical limiter in cases of southerly Föhn flow over the Alps showed a noticeable improvement of the predicted precipitation field. The spatial distribution of rain over mountainous areas appears to be much less noisy and the peak values over mountain tops are significantly reduced compared to the reference runs with standard 4th-order horizontal diffusion. Also, the dry valley effect is removed and the model's tendency for blocking frontal precipitation north of the Alps is weakened.

Parallel test experiments with the modified horizontal diffusion scheme have been conducted at MeteoSwiss and at DWD for longer time periods. The statistical evaluation against observed surface weather parameters revealed a neutral impact of the new smoothing scheme to most parameters, but a beneficial impact to the predicted precipitation, especially in mountainous areas.

Acknowledgements

Thanks to all colleagues who contributed to this work: J.-M Bettems implemented and supported the test suite at MetoSwiss, F. Schubiger did the statistical evaluation at MeteoSwiss, T. Hanisch supported the experimental test suite at DWD and U. Damrath did the statistical evaluation at DWD. Special thanks to A. Gassmann and D. Majewski for discussions and helpful suggestions.

References

Gassmann, A., 2001: Filtering of LM-Orography. *COSMO Newsletter*, No.1, 71-78.

Raymond, W.H., 1988: High-order low-pass implicit tangent filters for use in finite area calculations. *Mon. Wea. Rev.*, **116**, 2132-2141.

Shapiro, R., 1975: Linear filtering. *Math. Comp.*, **29**, 1094-1097.

Smolarkiewicz, P.K., 1989: Comment on "A positive definite advection scheme obtained by nonlinear renormalization of the advective fluxes". *Mon. Wea. Rev.*, **117**, 2626-2632.

Xue, M., 2000: High-Order Monotonic Numerical Diffusion and Smoothing. *Mon. Wea. Rev.*, **128**, 2853-2864.

Zalesak, S.T.,1979: Fully multidimensional flux-corrected transport algorithms for fluids. *J. Comp. Phys.*, **31**, 335-362.

Zängl, G., 2000: A modified temperature diffusion scheme for simulations over complex terrain and its application to idealized Foehn simulations. *MAP Newsletter*, No. 13.

List of COSMO Newsletters and Technical Reports

(available for download from the COSMO Website: www.cosmo-model.org)

COSMO Newsletters

Newsletter No.1, February 2001.

COSMO Technical Reports

No. 1, Dmitrii Mironov and Matthias Raschendorfer (2001): *Evaluation of Empirical Parameters of the New LM Surface-Layer Parameterization Scheme. Results from Numerical Experiments Including the Soil Moisture Analysis.*

No. 2, Reinhold Schrodin and Erdmann Heise (2001): *The Multi-Layer Version of the DWD Soil Model TERRA_LM.*

No. 3, Günther Doms (2001): *A Scheme for Monotonic Numerical Diffusion in the LM.*

COSMO Technical Reports

Issues of the COSMO Technical Reports series are published by the *Consortium for Small-Scale Modelling* at non-regular intervals. COSMO is a European group for numerical weather prediction with participating meteorological services from Germany (DWD, AWGeophys), Greece (HNMS), Italy (UGM, ARPA-SMR) and Switzerland (MeteoSwiss). The general goal is to develop, improve and maintain a non-hydrostatic limited area modelling system to be used for both operational and research applications by the members of COSMO. This system is initially based on the Lokal-Modell (LM) of DWD with its corresponding data assimilation system.

The Technical Reports are intended

- for scientific contributions and a documentation of research activities,
- to present and discuss results obtained from the model system,
- to present and discuss verification results and interpretation methods,
- for a documentation of technical changes to the model system,
- to give an overview of new components of the model system.

The purpose of these reports is to communicate results, changes and progress related to the LM model system relatively fast within the COSMO consortium, and also to inform other NWP groups on our current research activities. In this way the discussion on a specific topic can be stimulated at an early stage. In order to publish a report very soon after the completition of the manuscript, we have decided to omit a thorough reviewing procedure and only a rough check is done by the editors and a third reviewer. We apologize for typographical and other errors or inconsistencies which may still be present.

At present, the Technical Reports are available for download from the COSMO web site (www.cosmo-model.org). If required, the member meteorological centres can produce hard-copies by their own for distribution within their service. All members of the consortium will be informed about new issues by email.

For any comments and questions, please contact the editors:

Günther Doms
guenther.doms@dwd.de

Ulrich Schättler
ulrich.schaettler@dwd.de